

UC Irvine

UC Irvine Previously Published Works

Title

Non-contact electroacoustic tomography with optical interferometer for electroporation therapy monitoring

Permalink

<https://escholarship.org/uc/item/547549m2>

Journal

Applied Physics Letters, 126(2)

ISSN

0003-6951

Authors

Xu, Yifei

Song, Yuchen

Sun, Leshan

et al.

Publication Date

2025-01-13

DOI

10.1063/5.0244192








Copyright Information

This work is made available under the terms of a Creative Commons Attribution License, available at <https://creativecommons.org/licenses/by/4.0/>

Peer reviewed

RESEARCH ARTICLE | JANUARY 17 2025

Non-contact electroacoustic tomography with optical interferometer for electroporation therapy monitoring

Yifei Xu ; Yuchen Song ; Leshan Sun ; Zhongping Chen  ; Liangzhong Xiang  

 Check for updates

Appl. Phys. Lett. 126, 023704 (2025)

<https://doi.org/10.1063/5.0244192>



Articles You May Be Interested In

Recent progress in multi-channel laser-ultrasonic receivers

AIP Conference Proceedings (May 2012)

A coupled model of electroporation and electrodeformation considering dynamic Young's modulus

Appl. Phys. Lett. (November 2023)

Experimental comparison of sonoporation and electroporation in cell transfection applications

ARLO (April 2004)



Applied Physics Letters

Special Topics Open for Submissions

[Learn More](#)



Non-contact electroacoustic tomography with optical interferometer for electroporation therapy monitoring

Cite as: Appl. Phys. Lett. **126**, 023704 (2025); doi: [10.1063/5.0244192](https://doi.org/10.1063/5.0244192)

Submitted: 16 October 2024 · Accepted: 4 January 2025 ·

Published Online: 17 January 2025



View Online



Export Citation



CrossMark

Yifei Xu,¹  Yuchen Song,^{1,2}  Leshan Sun,¹  Zhongping Chen,^{1,2,a)}  and Liangzhong Xiang^{1,2,3,a)} 

AFFILIATIONS

¹Department of Biomedical Engineering, University of California, Irvine, California 92617, USA

²Beckman Laser Institute & Medical Clinic, University of California, Irvine, Irvine, California 92612, USA

³Department of Radiological Sciences, University of California, Irvine, California 92697, USA

^{a)}Authors to whom correspondence should be addressed: z2chen@uci.edu and liangzhx@hs.uci.edu

ABSTRACT

Electroacoustic imaging is an imaging modality used to detect electric field energy distribution during electroporation, offering valuable guidance for clinical procedures, particularly in deep tissues. Traditionally, single-element piezoelectric transducers or arrays have been employed for this purpose. However, these piezoelectric sensors are sensitive to electromagnetic interference and require physical contact with the sample through a coupling medium, raising concerns for both clinical and preclinical applications. To overcome these limitations, a multi-channel random quadrature ultrasonics system has been developed, enabling non-contact detection of electroacoustic signals. In this study, we demonstrated that this non-contact technique effectively detects electroacoustic signals, identifies electroporation regions, and reconstructs electric energy distribution, offering a promising approach for monitoring electroporation therapy.

Published under an exclusive license by AIP Publishing. <https://doi.org/10.1063/5.0244192>

The application of electric fields in medical treatments has a long history of development.^{1,2} Numerous studies have reported the use of electric fields in areas such as cancer treatment,³ tissue engineering,⁴ and wound healing.⁵ Among these, electroporation has gained significant attention due to its widespread applications in tumor ablation,⁶ drug delivery,⁷ and deoxyribonucleic acid (DNA) transfection.⁸ Electroporation is a technique that uses pulsed electric fields (PEF) to create pores in the cell membrane. When short, high-intensity pulses are applied to tissue, the permeability of the cell membrane increases due to pore formation. In reversible electroporation (RE), the cell membrane recovers after a period of time. However, when the pulse parameters (voltage, pulse width, etc.) are too strong, the cell cannot maintain homeostatic and lead to cell death, a process known as irreversible electroporation (IRE).

Traditional electroporation techniques use pulse widths ranging from hundreds of microseconds to several milliseconds, but recently, electroporation induced by nanosecond pulsed electric fields (nsPEF) has attracted attention.^{9,10} Compared to conventional electroporation protocols, nsPEF-induced electroporation offers advantages such as reduced thermal effects and minimized muscle contractions.^{11,12} Several studies have demonstrated its

effective use in immunotherapy and cancer treatment.^{13–15} Current electroporation treatment protocols often depend on numerical simulations, with post-operative assessments relying on magnetic resonance imaging (MRI), ultrasound, and other imaging modalities.¹⁶ However, there is a need for a method that enables real-time detection during the procedure. To address this, we propose electroacoustic tomography (EAT) as an intraoperative imaging technique to detect the treatment area.¹⁷

Electroacoustic tomography (EAT) is a noninvasive, label-free, and non-radiative imaging technique that uses ultrasound signals to map electric field distribution within tissues, based on their absorption of nsPEF energy. Traditional acoustic imaging systems rely on piezoelectric ultrasound transducer, which require coupling media like water or ultrasound gel.¹⁸ However, in specific clinical situations, such as burn injuries or during surgery, direct contact with the coupling medium should be minimized or avoided.¹⁸ Meanwhile, piezoelectric transducers are sensitive to electromagnetic interference (EMI), and the detection sensitivity drops as the size of piezoelectric elements is reduced.¹⁹

As an alternative method, optical methods have been developed by measuring surface displacement induced by thermoacoustic effect

and shock wave propagation.^{20,21} Compared to piezoelectric sensors, the sensitivity of optical sensing is independent of its size, which is less sensitive to EMI and some of them allow non-contact measurement. Recently, several studies have been reported to use optical methods to detect electroacoustic signals including probe beam deflection (PBD),²² optical spectroscopy,²³ and coherent anti-stokes Raman scattering and micro-spectroscopy (CARS).²⁴ However, these methods are usually applied for cellular level study, which hinders its clinical application.

In this paper, we propose to use the multi-channel random quadrature (MCRQ) interferometer to remotely detect the electroacoustic signal generated during electroporation.²⁵ The EA signal is generated by two clinical needle electrodes inserted in agarose based phantom and potato phantom with different electrical parameters. The results show that this method effectively reflects changes in the electrical parameters of electroporation and demonstrates the ability to identify the IRE ablated region. A two-dimensional (2D) EAT image was obtained through rotational scanning, with the results aligning well with those previously obtained using conventional ultrasound piezoelectric transducers.²⁶

Electroacoustic tomography detects electric fields in soft tissues by inducing acoustic pressure with high-voltage pulses. When both thermal and stress constraints are satisfied, thermal diffusion and stress propagation in the tissue during pulse delivery are negligible. Therefore, the initial acoustic pressure can be expressed as¹⁷

$$p_0(r, t) = \frac{\beta(r)\sigma(r)}{\kappa(r)\rho(r, t)C_v(r)} E(r)^2 g(t), \quad (1)$$

where $\beta(r)$ is the thermal coefficient, $\sigma(r)$ denotes the specific electrical conductivity, $\kappa(r)$ is the isothermal compressibility, $\rho(r, t)$ is the mass density, and $C_v(r)$ denotes the specific heat capacity at constant volume. $E(r)$ is the electric field strength at point r , and $g(t)$ is the duration of the electric pulse.

The excitation of acoustic signals induced by the thermoelastic expansions of the tissue can be described by wave equations and then solved by Green's functions. The acoustic pressure at position r and time t can be described as¹⁷

$$p(r, t) = \frac{1}{4\pi v_s^2} \int dr' \frac{1}{|r-r'|} p_0(r') \delta\left(t - \frac{|r-r'|}{v_s}\right). \quad (2)$$

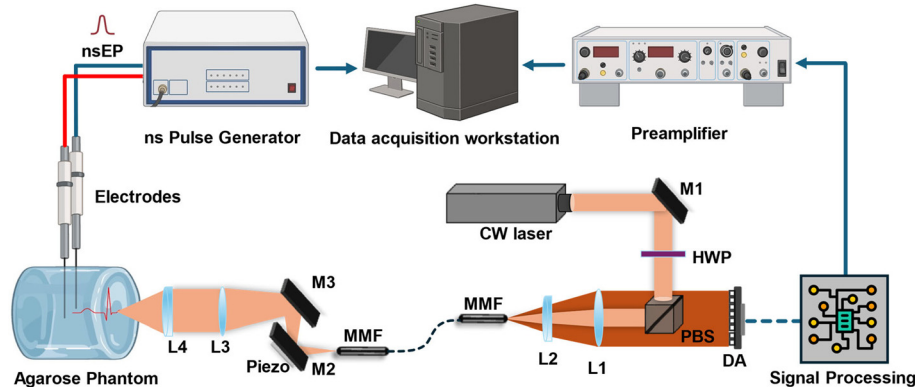


FIG. 1. Schematic of MCRQ interferometer based EAT system. M1–M3: mirror; HWP: half-wave plate; PBS: polarization beam splitter; L1–L4: lens; MMF: multi-mode fiber; Piezo: piezo actuator; and DA: multi-channel detector array.

The relationship between electroacoustic pressure and sample displacement can be expressed as follows:

$$\rho \frac{\partial^2}{\partial t^2} d(r, t) = -\nabla p(r, t), \quad (3)$$

where vector d is the sample displacement induced by electroacoustic pressure. The displacement will change the phase of backscattered signals which after interfering with reference beam can be detected by a photon detector array,

$$I^n = I_{ref}^n + I_{obj}^n + 2\sqrt{I_{ref}^n * I_{obj}^n} * \cos[\theta^n(t) + \varphi_{ea}(t)], \quad (4)$$

where I^n is the interference signal detected by detector array, I_{ref}^n and I_{obj}^n are the intensity of reference beam and object beam, θ^n is the initial phase of random speckle, and φ_{ea} is the phase variation induced by electroacoustic pressure. After linear demodulation to recover the displacement direction,²⁷ the phase change can be retrieved by the processed output signal V_{out} ,

$$V_{out} = \varphi_{ea}(t) * 2 \sum_n \sqrt{I_{ref}^n * I_{obj}^n} * \sin(\theta^n(t)). \quad (5)$$

Therefore, we can obtain the intensity of electric field energy information in tissue through the output signal.

To validate the effectiveness of our optical interferometer system in detecting EA signals, we constructed the experimental setup as shown in Fig. 1. The system is divided into two parts: (1) EA signal excitation and (2) optical detection part. For signal excitation session, a custom nanosecond pulse generator was used to deliver the electrical pulses. The generator allows for adjustable voltage (0–2000 V), pulse width (100 ns–100 μ s), and repetition frequency (1–1 MHz), enabling customized treatment protocols. The generated electrical pulses were delivered to two clinical needle electrodes with a diameter of 1 mm and adjustable exposed length (AngioDynamics, 20400107), which were inserted into the phantom to induce the electroacoustic signal. As to the optical detection part, the MCRQ interferometer consists of two primary components: the optical head and a compact Modulo receiver, connected by a multimode fiber. In the compact quartet receiver, a 30 mW continuous-wave (CW) laser with a wavelength of 1064 nm is employed for the interrogation system. A 24 channel detector array is utilized to detect interference signals. The multimode fiber delivers the incident laser beam to the optical head and collects the backscattered

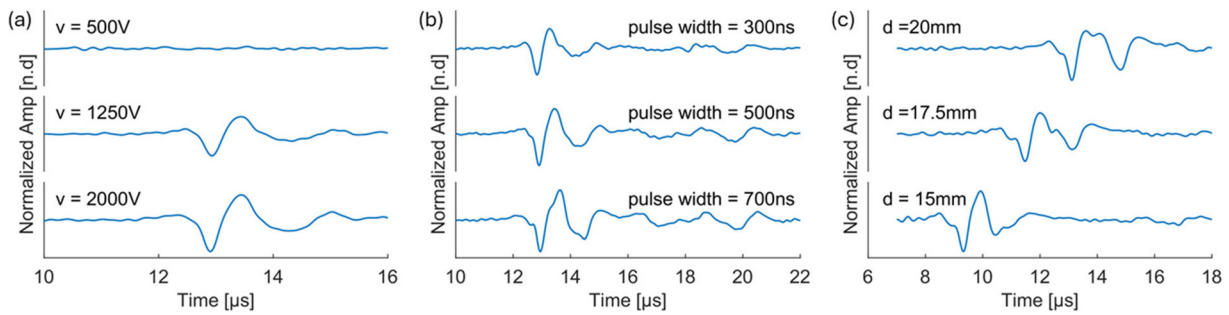


FIG. 2. Electroacoustic signals detected by the MCRQ interferometer at different parameter settings. The EA signal increases with increasing (a) pulse voltage and (b) pulse width; (c) the time-of-flight of the EA signal decreases with decreasing distance from the electrodes to the phantom surface. All results were averaged 200 times.

object beam from the optical head. Within the optical head, a piezo actuator at 330 kHz is used for signal calibration and to implement linear demodulation at 400 kHz. The signal processing mainly involves linear demodulation, which uses logic switches to accurately recover the displacement direction.²⁷ The output signal is amplified by 60 dB (JSR Ultrasonics, DPR 300, Japan) and detected using an oscilloscope (Tektronix Inc., MSO54B, USA).

To demonstrate the performance of the system, a 1% agarose phantom was tested with different electric pulse parameters. To provide the necessary conductivity and scattering properties for imaging, 1% sodium chloride and 1% intralipid were added. The exposed distance of the electrodes was set to 10 mm, and they were inserted laterally into the cylindrical phantom until the exposed portion of the electrodes was positioned at the center of the phantom. The detection beam of the interferometer was focused on the top surface of the phantom. We initially examined the effect of pulse voltage on the detected signals. The output voltage was set to 500, 1250, and 2000 V, with a pulse width of 500 ns and at a frequency of 50 Hz. The average denoised signals are presented in Fig. 2(a). As shown, no significant

signal was detected at 500 V, but as the voltage increased, the amplitude of the detected signals rose accordingly. Next, we fixed the voltage at 2000 V and varied the pulse width to 300, 500, and 700 ns at 50 Hz. The average denoised signals are shown in Fig. 2(b). As the pulse width increased, the energy per pulse increased, resulting in a stronger detected signal. These two sets of experiments demonstrate that the detected signal can clearly reflect the dosage of the electrical pulses. Figure 2(c) shows signal's time of flight varied with the electrode depth reference with sample surface. The distance between electrodes and phantom surface was gradually decreased by 2.5 mm. The calculated signal propagation speed was approximately 1500 m/s, similar to the speed of ultrasound in water.

Next, we performed scans on agarose and potato phantom [Fig. 3(a)] to obtain the distribution of EA signal intensity across the surface of the phantoms. Potato is a commonly used plant model for evaluating the ablation regions in IRE.²⁸ The agarose phantom used in this experiment had the same specifications as the one used in the experiments described in Fig. 2. The electrical pulses were delivered at 500 ns pulse width and 50 Hz repetition rate at 1500 and 2000 V for

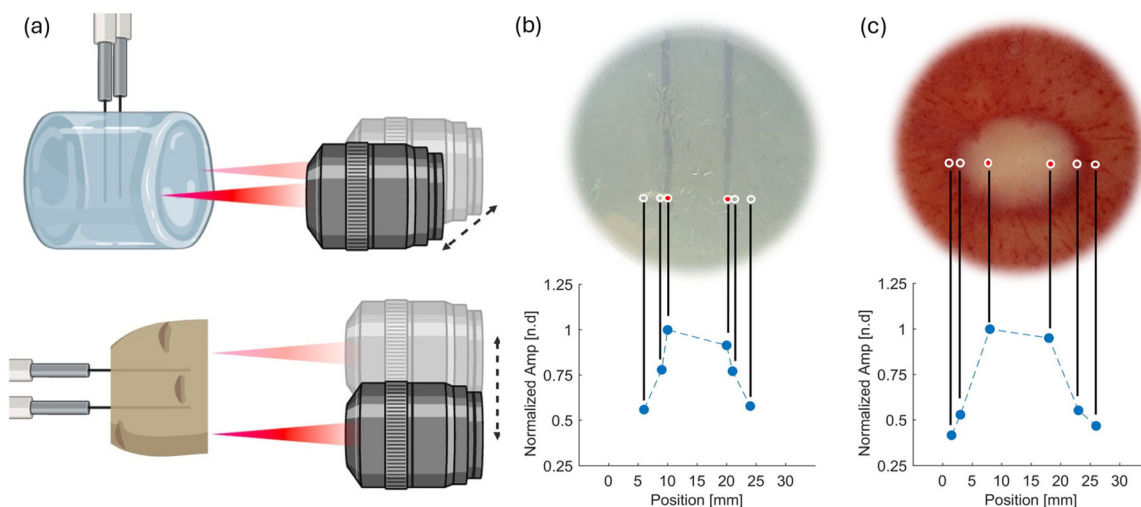


FIG. 3. EA signal intensity distribution on the surface of the phantom. (a) Scanning path of the beam (dashed arrows) and electrode arrangement. (b) and (c) The photographs and signal scanning points of the agarose and potato models, and the line graph below shows the EA signal contours obtained from the scans. The scans show that the intensity of the signal is strongest around the electrodes and decreases as one moves away from the electrodes. All results were averaged 200 times.

agarose and potato phantom, respectively. After applying the electrical pulses, we cut 5 mm potato phantom from the treatment area. The slices were then immersed in 50 ml of 1% 2,3,5-triphenyltetrazolium chloride (TTC) solution for 3 h of staining to compare the results with the EA signal scan. The use of TTC stain on the potato provides a faster and more accurate assessment.²⁹ The dehydrogenase produced by cell mitochondria reduces TTC to insoluble red triphenylformazan crystals, which causes the non-ablated areas to appear red, while the unstained white regions can be identified as IRE ablation zones as shown in Fig. 3(c).

The EA signal intensity of agarose and potato phantom is shown in Figs. 3(b) and 3(c), respectively. The white circles in the figure indicate the positions where signals were acquired, with the red-filled circles representing the locations where the signals were captured directly in front of the electrodes. It was observed that the signal strength was highest at the electrodes and significantly decreases as the detection point moves away from them. The distribution of the EA signal intensity profile is similar for both agarose and potato phantom, and the signal intensity dropped by approximately 50% within a 5 mm distance, indicating that the energy of the electrical field attenuates rapidly as it propagates. When the signal strength dropped below approximately 50% of the maximum detected EA signal intensity, only irreversible electroporation or no electroporation occurred.

Next, to demonstrate the imaging capabilities of our system, we set up the imaging system as shown in Fig. 4(a). In this setup, a 1% saline solution was used to induce the EA signal. One side of the water tank was opened and covered with polyvinyl chloride (PVC) film, on which the detection beam was focused. Meanwhile, the focused beam path crosses the electrodes rotation axis. The electrodes with 10 mm spacing were fixed on a rotating platform and rotated along the central axis of

the electrodes. The rotation angle was set to 3 degrees, with a total of 120 steps to scan all viewing angles. The electrodes output 1500 V, 500 ns pulses, and at each angle, 100 pulses were averaged for denoising.

Figure 4(b) shows the signals collected at rotation angles of 0, 45, and 90 degrees. It can be observed that the signals from the two electrodes gradually converge as the rotation proceeds, eventually overlapping into a single signal. This indicates that the system can capture not only the variations in signal strength but also depth of the electric field. As shown in Fig. 4(c), we used a back-projection algorithm to reconstruct a two-dimensional image from the signals collected at all angles.³⁰ The distance between the two reconstructed hotspots is approximately 10 mm, which is consistent with the spacing of electrodes. The signal intensity is strongest at the center and gradually decreases with the location away from center. In addition, we performed a physical simulation (COMSOL Multiphysics 6.0, Sweden), and the resulting electric field streamlines were overlapped onto the reconstructed image. The arrows represent the direction of the electric field. Figure 4(d) shows a profile line extracted along the dashed line in Fig. 4(c). The results are consistent with our previous work.^{17,31}

Current electroporation treatment plans are often developed through simulations, lacking real-time monitoring capabilities, which significantly limits their advancement. The introduction of electroacoustic tomography (EAT) offers a potential solution for real-time monitoring during electroporation treatments. In previous studies, EAT imaging systems were built using piezoelectric transducers, but the requirement for physical contact and coupling media restricted their broader clinical application. The MCRQ interferometer based EAT system offers a non-contact monitoring solution to this limitation, simplifying clinical workflows while reducing the risk of infection for special populations such as infants and individuals with sensitive

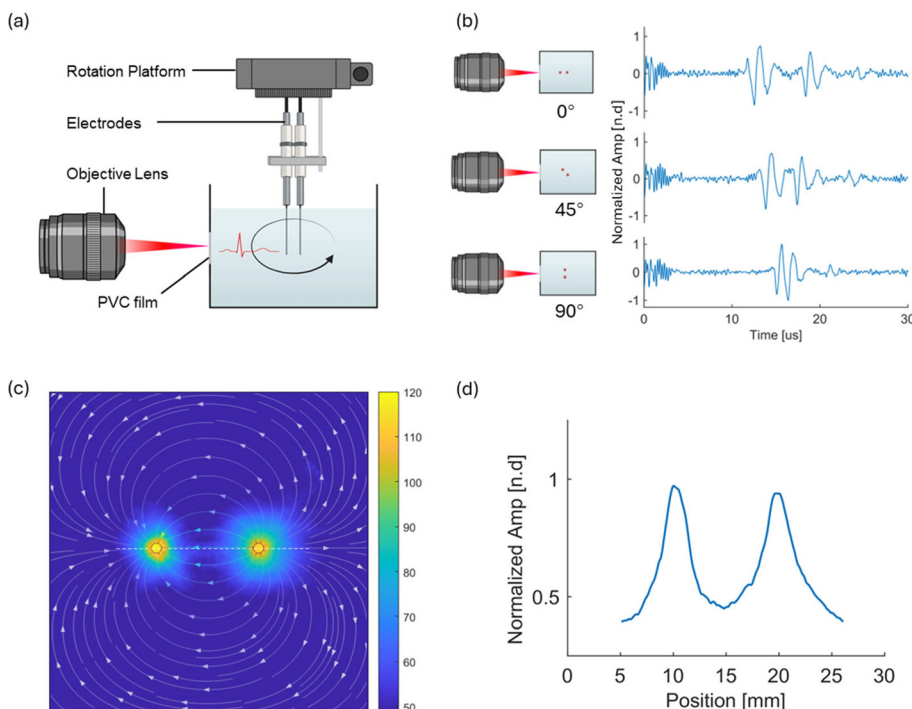


FIG. 4. 2D EAT reconstruction image with rotation platform. (a) Experiment setup. (b) EA signal at different rotation angles. (c) Reconstructed 2D EAT image. (d) The image profile along with the white dash line.

skin.³² The results demonstrate that the system can effectively detect EA signals generated in deep tissues and has the potential to provide real-time feedback on treatment outcomes.

Since the detected EA signal correlates with the intensity of the electrical pulse energy within the tissue, it is possible to estimate the energy distribution at different locations during IRE treatment, which can further help with the assessment of tissue ablation. In the potato phantom experiment, the intensity of the detected EA signal correlated with the ablation area. Although the number of scanning points is limited, the signal intensity at even a single location can be valuable. For example, when control of the ablation area is critical, monitoring points may be placed near important tissues to ensure that they are not affected. Similarly, in cases where the electrode spacing is large, placing the monitoring point in the center helps to avoid incomplete ablation. Limited by the sensitivity of the system, we delivered 200 pulses at each detection point in the phantom for averaging. Although the number of pulses affects the ablation range, the effect is small when the total number of pulses is high, and therefore has a small effect on the ablation range.³³

The proposed MCRQ interferometer detection system provides signals with detailed information, offering the potential to capture electric field data from deep tissues in a noncontact manner. Unlike conventional interferometer systems, the MCRQ employs a multimode fiber to collect more backscattered signals, and its multichannel detector array enhances performance on uneven surfaces. A 330 kHz piezo actuator is employed for signal calibration to compensate phase change for uneven surfaces and minor vibrations. However, several limitations still require improvement. One challenge with laser interferometry is its sensitivity to temperature fluctuations and vibrations, which can reduce both sensitivity and detection range. Additionally, the noise equivalent power of the optical detection system is higher compared to conventional piezoelectric transducers, making it difficult to detect EA signals induced by low-power electrical pulses. That is why hundreds of averages are needed to get a high signal noise ratio (SNR) EA signal, which limits the imaging speed of the system.

Limited by the sensitivity of our system, hundreds of electrical pulses are needed for averaging. The signal intensity is affected by the electrodes spacing, the distance between sample surface and electrodes tips, and alignment between light scanning beam and exposed electrodes tips. In addition to the electrodes alignment, the system noise suppression in the experiment is also crucial. The strong electric field brought by the high-voltage pulse will cause interference to the circuitry of the instrument, and electromagnetic shielding of the wires and instruments can effectively reduce electromagnetic interference (EMI). To improve the performance of MCRQ interferometer, more channels for detector array are needed to enhance signal averaging without extending the acquisition time. Some optical resonators could also further increase system sensitivity compared to traditional interference system.^{34–36} Furthermore, defocusing of the detection beam can decrease sensitivity and result in inaccurate measurements. In addition to the hardware system part, some more efficient post-processing noise reduction methods, such as wavelet denoising and deep learning based signal enhancement methods, have been reported to significantly improve the signal processing speed of the system to significantly improve the signal processing speed of the system.^{26,37}

In summary, an ultrasound signal acquisition system was developed and validated for the non-contact assessment of electroporation

treatment in deep tissues. EA signals, which varied with treatment parameters, were detected in both agarose phantoms and potato phantoms using the MCRQ interferometer system. A 2D distribution of electric field energy in saline was obtained through rotate scanning. Since electroporation treatment outcomes are significantly influenced by pulse parameters, the real-time EA signals and their reconstructed images were shown to reflect these variations, offering a potential method to guide electroporation treatments. The non-contact EA signal acquisition capability of the MCRQ interferometer-based system eliminates the need for physical contact via coupling media, which is non-sensitive to EMI, thereby enhancing the clinical applicability of this technology.

We are pleased to thank Sound&Bright for providing technical support for the multi-channel random quadrature interferometer.

This work was supported by the National Institutes of Health (Nos. R37CA240806, U01CA288351, R50CA283816, R01HL125084, and R01EB030024). The authors would like to acknowledge the support from UCI Chao Family Comprehensive Cancer Center (No. P30CA062203).

AUTHOR DECLARATIONS

Conflict of Interest

The authors have no conflicts to disclose.

Author Contributions

Yifei Xu and Yuchen Song contributed equally to this paper.

Yifei Xu: Conceptualization (equal); Data curation (equal); Formal analysis (equal); Investigation (equal); Methodology (equal); Visualization (equal); Writing – original draft (equal); Writing – review & editing (equal). **Yuchen Song:** Conceptualization (equal); Data curation (equal); Formal analysis (equal); Investigation (equal); Methodology (equal); Validation (equal); Writing – original draft (equal); Writing – review & editing (equal). **Leshan Sun:** Formal analysis (supporting); Visualization (supporting). **Zhongping Chen:** Conceptualization (equal); Project administration (equal); Supervision (equal); Writing – review & editing (equal). **Liangzhong Xiang:** Conceptualization (equal); Funding acquisition (equal); Project administration (equal); Supervision (equal); Writing – review & editing (equal).

DATA AVAILABILITY

The data that support the findings of this study are available from the corresponding authors upon reasonable request.

REFERENCES

- ¹H. A. Whitaker, C. U. M. Smith, and S. Finger, *Brain, Mind, and Medicine: Essays in Eighteenth-Century Neuroscience* (Springer, New York, NY, 2007).
- ²F. X. Hart and J. R. Palisano, *The Application of Electric Fields in Biology and Medicine* (InTech, 2018).
- ³D. Fabian, M. D. P. Guillermo Prieto Eibl, I. Alnahhas, N. Sebastian, P. Giglio, V. Puduvali, J. Gonzalez, and J. D. Palmer, “Treatment of glioblastoma (GBM) with the addition of tumor-treating fields (TTF): A review,” *Cancers* **11**, 174 (2019).
- ⁴C. N. M. Ryan, M. N. Doulgeroglou, D. I. Zeugolis, C. N. M. Ryan, M. N. Doulgeroglou, and D. I. Zeugolis, “Electric field stimulation for tissue engineering applications,” *BMC Biomed. Eng.* **3**, 1–9 (2021).

- ⁵M. A. Messerli and D. M. Graham, "Extracellular electrical fields direct wound healing and regeneration," *Biol. Bull.* **221**, 79 (2011).
- ⁶H. J. Scheffer, K. Nielsen, M. Jong, A. Tilborg, J. M. Vieveen, A. R. A. Bouwman, S. Meijer, C. Kuijk, P. Tol, and M. R. Meijerink, "Irreversible electroporation for nonthermal tumor ablation in the clinical setting: A systematic review of safety and efficacy," *J. Vasc. Interventional Radiol.* **25**, 997 (2014).
- ⁷N. Bhutiani, S. Agle, Y. Li, S. Li, and R. C. G. Martin, "Irreversible electroporation enhances delivery of gemcitabine to pancreatic adenocarcinoma," *J. Surg. Oncol.* **114**, 181 (2016).
- ⁸A. Taketo, "DNA transfection of *Escherichia coli* by electroporation," *Biochim. Biophys. Acta (BBA) - Gene Struct. Expression* **949**, 318 (1988).
- ⁹J. C. Weaver, "Electroporation theory. Concepts and mechanisms," *Methods Mol. Biol.* **55**, 3–28 (1995).
- ¹⁰A. R. Ruiz-Fernández, L. Campos, S. E. Gutierrez-Maldonado, G. Núñez, F. Villanelo, T. Perez-Acle, A. R. Ruiz-Fernández, L. Campos, S. E. Gutierrez-Maldonado, G. Núñez, F. Villanelo, and T. Perez-Acle, "Nanosecond pulsed electric field (nsPEF): Opening the biotechnological Pandora's box," *Int. J. Mol. Sci.* **23**, 6158 (2022).
- ¹¹E. Gudvangen, V. Kim, V. Novickij, F. Battista, A. G. Pakhomov, E. Gudvangen, V. Kim, V. Novickij, F. Battista, and A. G. Pakhomov, "Electroporation and cell killing by milli- to nanosecond pulses and avoiding neuromuscular stimulation in cancer ablation," *Sci. Rep.* **12**, 1763 (2022).
- ¹²C. Valdez, M. B. Jirjis, C. A. Roth, R. A. Barnes, B. L. Ibey, C. Valdez, M. B. Jirjis, C. C. Roth, R. A. Barnes, and B. L. Ibey, "Nanosecond electric pulses modulate skeletal muscle calcium dynamics and contraction," *Proc. SPIE* **10066**, 100660X (2017).
- ¹³T. F. Justesen, A. Orhan, H. Raskov, C. Nolsoe, and I. Gögenur, "Electroporation and immunotherapy—Unleashing the abscopal effect," *Cancers* **14**, 2876 (2022).
- ¹⁴A. Vizintin, S. Marković, J. Ščančar, and D. Miklavčič, "Electroporation with nanosecond pulses and bleomycin or cisplatin results in efficient cell kill and low metal release from electrodes," *Bioelectrochemistry* **140**, 107798 (2021).
- ¹⁵M. Xu, D. Xu, G. Dong, Z. Ren, W. Zhang, T. Aji, Q. Zhao, X. Chen, and T. Jiang, "The safety and efficacy of nanosecond pulsed electric field in patients with hepatocellular carcinoma: A prospective phase 1 clinical study protocol," *Front. Oncol.* **12**, 869316 (2022).
- ¹⁶M. Silk, D. Tahour, G. Srimathveeravalli, S. B. Solomon, and R. H. Thornton, "The state of irreversible electroporation in interventional oncology," *Semin. Interventional Radiol.* **31**, 111 (2014).
- ¹⁷Y. Xu, L. Sun, S. Wang, Y. Yan, P. Pandey, V. Novickij, L. Xiang, Y. Xu, L. Sun, S. Wang, Y. Yan, P. Pandey, V. Novickij, and L. Xiang, "Electroacoustic tomography for real-time visualization of electrical field dynamics in deep tissue during electroporation," *Commun. Eng.* **2**(1), 75 (2023).
- ¹⁸Z. Hosseinaee, M. Le, K. Bell, and P. H. Reza, "Towards non-contact photoacoustic imaging [review]," *Photoacoustics* **20**, 100207 (2020).
- ¹⁹J. Sirohi and I. Chopra, "Fundamental understanding of piezoelectric strain sensors," *J. Intell. Mater. Syst. Struct.* **11**, 246–257 (2000).
- ²⁰J. W. Wagner, "Optical detection of ultrasound," *Phys. Acoust.* **19**, 201–266 (1990).
- ²¹G. Wissmeyer, M. A. Pleitez, A. Rosenthal, and V. Ntziachristos, "Looking at sound: Optoacoustics with all-optical ultrasound detection," *Light-Sci. Appl.* **7**, 53 (2018).
- ²²R. A. Barnes, C. C. Roth, H. T. Beier, G. Noojin, C. Valdez, J. Bixler, E. Moen, M. Shadaram, and B. L. Ibey, "Probe beam deflection optical imaging of thermal and mechanical phenomena resulting from nanosecond electric pulse (nsEP) exposure," *Opt. Express* **25**, 6621–6643 (2017).
- ²³C. Merla, M. Liberti, P. Marracino, A. Muscat, A. Azan, F. Apollonio, L. M. Mir, C. Merla, M. Liberti, P. Marracino, A. Muscat, A. Azan, F. Apollonio, and L. M. Mir, "A wide-band bio-chip for real-time optical detection of bioelectromagnetic interactions with cells," *Sci. Rep.* **8**, 5044 (2018).
- ²⁴C. Merla, M. Nardoni, M. Scherfan, S. Petralito, L. Caramazza, F. Apollonio, M. Liberti, P. Paolicelli, B. Attal-Tretout, and L. M. Mir, "Changes in hydration of liposome membranes exposed to nanosecond electric pulses detected by wide-field coherent anti-stokes Raman microspectroscopy," *Bioelectrochemistry* **147**, 108218 (2022).
- ²⁵B. Pouet, S. Breugnot, and P. Clémenceau, "Robust laser-ultrasonic interferometer based on random quadrature demodulation," *AIP Conf. Proc.* **820**, 233–239 (2006).
- ²⁶Z. Jiang, Y. Xu, L. Sun, S. Srinivasan, Q. J. Wu, L. Xiang, and L. Ren, "Enhanced electroacoustic tomography with supervised learning for real-time electroporation monitoring," *Precis. Radiat. Oncol.* **8**, 110 (2024).
- ²⁷B. Pouet, A. Wartelle, and S. Breugnot, "Multi-channel random-quadrature receiver for industrial laser-ultrasonics," in *2011 IEEE International Ultrasonics Symposium* (IEEE, 2011).
- ²⁸Y. Zhao, H. Liu, S. P. Bhonsle, Y. Wang, R. V. Davalos, C. Yao, Y. Zhao, H. Liu, S. P. Bhonsle, Y. Wang, R. V. Davalos, and C. Yao, "Ablation outcome of irreversible electroporation on potato monitored by impedance spectrum under multi-electrode system," *Biomed. Eng. Online* **17**, 1–13 (2018).
- ²⁹S. Jeong, H. Kim, J. Park, K. W. Kim, S. B. Sim, J. H. Chung, S. Jeong, H. Kim, J. Park, K. W. Kim, S. B. Sim, and J. H. Chung, "Evaluation of electroporated area using 2,3,5-triphenyltetrazolium chloride in a potato model," *Sci. Rep.* **11**, 20431 (2021).
- ³⁰M. Xu and L. V. Wang, "Universal back-projection algorithm for photoacoustic computed tomography," *Phys. Rev. E* **71**, 016706 (2005).
- ³¹M. Wang, A. Zarafshani, P. Samant, J. Merrill, D. Li, and L. Xiang, "Feasibility of electroacoustic tomography: A simulation study," *IEEE Trans. Ultrason. Ferroelectr. Freq. Control* **67**, 889 (2020).
- ³²X. Zhang, J. R. Fincke, C. M. Wynn, M. R. Johnson, R. W. Haupt, and B. W. Anthony, "Full noncontact laser ultrasound: First human data," *Light. Sci. Appl.* **8**, 119 (2019).
- ³³F. Guo, X. H. Gou, J. G. Sun, J. Hong, and Y. P. Zhang, "Modeling methods in overlapping electroporation treatments: Pulse number effects on tissue conductivity and ablation area," *Electrochim. Acta* **503**, 144883 (2024).
- ³⁴H. Li, B. Dong, Z. Zhang, H. F. Zhang, and C. Sun, "A transparent broadband ultrasonic detector based on an optical micro-ring resonator for photoacoustic microscopy," *Sci. Rep.* **4**, 4496 (2014).
- ³⁵A. Rosenthal, D. Razansky, and V. Ntziachristos, "High-sensitivity compact ultrasonic detector based on a pi-phase-shifted fiber Bragg grating," *Opt. Lett.* **36**, 1833–1835 (2011).
- ³⁶E. Zhang, J. Laufer, and P. Beard, "Backward-mode multiwavelength photoacoustic scanner using a planar Fabry-Perot polymer film ultrasound sensor for high-resolution three-dimensional imaging of biological tissues," *Appl. Opt.* **47**, 561–577 (2008).
- ³⁷R. van Bergen, L. Sun, P. K. Pandey, S. Wang, K. Bjegovic, G. Gonzalez, Y. Chen, R. Lopata, and L. Xiang, "Discrete wavelet transformation for the sensitive detection of ultrashort radiation pulse with radiation-induced acoustics," *IEEE Trans. Radiat. Plasma Med. Sci.* **8**, 76–87 (2024).